PLOS ONE

RESEARCH ARTICLE

Motor neuron activity enhances the proteomic stress caused by autophagy defects in the target muscle

Saurabh Srivastav, Kevin van der Graaf, Prisha C. Jonnalagadda, Maanvi Thawani, James A. McNew*, Michael Stern*

Department of BioSciences, Rice University, Houston, TX, United States of America

* mcnew@rice.edu (JAM); stern@rice.edu (MS)

Citation: Srivastav S, van der Graaf K, Jonnalagadda PC, Thawani M, McNew JA, Stern M (2024) Motor neuron activity enhances the proteomic stress caused by autophagy defects in the target muscle. PLoS ONE 19(1): e0291477. https://doi.org/10.1371/journal.pone.0291477

Editor: Krishna Moorthi Bhat, University South Florida College of Medicine, UNITED STATES

Received: August 28, 2023

Accepted: December 12, 2023

Published: January 2, 2024

Data Availability Statement: All relevant information for accessing the data necessary for replicating the study's results are included in the manuscript.

Funding: The study was funded by the National Institute of Neurological Disorders and Stroke (grants R01 NS102676 and R21 NS111340) to both MS and JAM. The funders had no role in study design, data collection and analysis, decision to publish, or preparation of the manuscript.

Abstract

Several lines of evidence demonstrate that increased neuronal excitability can enhance proteomic stress. For example, epilepsy can enhance the proteomic stress caused by the expression of certain aggregation-prone proteins implicated in neurodegeneration. However, unanswered questions remain concerning the mechanisms by which increased neuronal excitability accomplishes this enhancement. Here we test whether increasing neuronal excitability at a particular identified glutamatergic synapse, the Drosophila larval neuromuscular junction, can enhance the proteomic stress caused by mutations in the ER fusion/GTPase gene *atlastin* (*atl*). It was previously shown that larval muscle from the atl^2 null mutant is defective in autophagy and accumulates protein aggregates containing ubiquitin (poly-UB aggregates). To determine if increased neuronal excitability might enhance the increased proteomic stress caused by atl^2, we activated the *TrpA1*-encoded excitability channel within neurons. We found that TrpA1 activation had no effect on poly-UB aggregate accumulation in wildtype muscle, but significantly increased poly-UB aggregate number in atl^2 muscle. Previous work has shown that *atl* loss from either neuron or muscle increases muscle poly-UB aggregate number. We found that neuronal TrpA1 activation enhanced poly-UB aggregate number when *atl* was removed from muscle, but not from neuron. Neuronal TrpA1 activation enhanced other phenotypes conferred by muscle *atl* loss, such as decreased pupal size and decreased viability. Taken together, these results indicate that the proteomic stress caused by muscle *atl* loss is enhanced by increasing neuronal excitability.

Introduction

Autophagy defects leading to accumulation of protein aggregates, often containing ubiquitin, are hallmarks of several prominent neurodegenerative disorders such as Alzheimer's, Parkinson's, and Huntington's disease [1–3]. For example, mice defective in autophagy exhibit neurodegeneration [4, 5], whereas inducing autophagy via treatment with rapamycin could partially suppress aggregate formation in model systems [6, 7]. These data suggest that a

Competing interests: The authors have declared that no competing interests exist.

common feature of neurodegenerative disorders might be proteomic stress, caused by any number of cell stressors including expression of aggregation-prone proteins or inhibition of autophagy.

Proteomic stress likewise appears to be involved in the family of neurodegenerative disorders termed the "Hereditary Spastic Paraplegias" (HSPs), which are caused by mutations in any of at least 72 genes. These HSP mutations confer the common pathology of progressive spasticity and paralysis. These behaviors are likely due to degeneration of upper motor neurons, which synapse onto the lower motor neurons of the spinal cord. Analysis of several HSP genes implicate defective autophagy as a common causal factor. For example, the HSP genes *spastizin (SPG15)*, *strumpellin (SPG8)* and *Spatacsin (SPG11)* encode proteins critical for autophagy function [8–10]. In addition, the HSP gene *atlastin (SPG3A)* encodes an ER fusion/GTPase protein that binds to the autophagy inducer ULK1 to induce autophagosome formation [11]. Drosophila muscle lacking *atl* accumulates undegraded autophagy cargo as well as protein aggregates containing ubiquitin (poly-UB aggregates) and exhibits precocious degeneration [12, 13]. Taken together, these data raise the possibility that defective autophagy is a causal factor for protein aggregate accumulation and ultimately degeneration.

Several lines of evidence demonstrate a link between neurodegeneration and conditions such as epilepsy that increase neuronal excitability. For example, neurodegeneration can cause seizures [14] whereas decreasing Tau expression can suppress seizures [15]. Likewise, increasing neuronal excitability can exacerbate degeneration. For instance, tauopathy can be induced or enhanced by temporal lobe epilepsy or other conditions that increase neuronal excitability [16, 17]. Furthermore, hyperexcitability is observed early in Alzheimer's progression in both patients and in mouse models [18, 19]. One mechanism by which hyperexcitability could induce degeneration is increased synaptic activity and consequent glutamate toxicity [20–22]. However, the mechanisms linking neuronal excitability with proteomic stress and ultimately degeneration remain incompletely understood.

Here we examine the effects of increased neuronal excitability, accomplished by activating the heat-inducible TrpA1 cation channel [23] within motor neurons, on proteomic stress at the glutamatergic Drosophila larval neuromuscular junction. We found that motor neuron TrpA1 activation in otherwise wildtype larvae failed to induce poly-UB aggregate accumulation in target muscle. However, activating TrpA1 in motor neurons from atl^2 null larvae, as well as from larvae in which *atl* was knocked down in muscle, significantly enhanced accumulation of these poly-UB aggregates. Expressing a second excitability allele, a dominant-negative allele in the "*Shaker*" potassium channel gene Sh^{DN}, likewise enhanced poly-UB aggregate accumulation in atl^2 larval muscle. We conclude that increasing motor neuron excitability increases proteomic stress in the target muscle, which is revealed in muscle in which autophagy machinery is crippled by *atl* loss.

Materials and methods

Drosophila stocks and media

The following stocks were obtained from the Bloomington Drosophila stock center (BDSC, Bloomington, Indiana): The Foxo transcriptional reporter *4EBP-lacZ* (#9558), *UAS-Dcr-2* (#24650), the muscle Gal4 driver *24B-Gal4* (#1767), *Df(atl)/TbTM6* (#7948) *OK371-Gal4*, in which *Gal4* is inserted into the motor-neuron specific gene encoding the vesicular glutamate transporter (#26160) and *nSyb-LexA*, in which *Gal4* is inserted into the panneuronal *Synaptobrevin* gene *(attP2*, #51951*)*, *UAS-TrpA1* (*attP16*, #26263). Flies bearing *UAS-*Sh^{DN} were generously provided by Tim Mosca (Thomas Jefferson University), flies bearing *Aop-TrpA1* in the *VK05* site were generously provided by Gerry Rubin (Janelia HHMI) and Kristin Scott

(University of California, Berkeley). *UAS-atlRNAi* and atl^2 were described previously [24]. All fly stocks were maintained on standard cornmeal/agar media as previously described [25]. All larvae were collected for imaging at the wandering third instar stage. For experiments shown in Figs 1–4 and in all supplemental figures, larvae were reared at 28˚ C for all stages. For experiments shown in Figs 5 and 6, eggs were collected and reared for two days at room temperature, then transferred to 28˚ C until they were collected for analysis. For experiments shown in Fig 7, larvae were reared at room temperature (21˚ C -22˚ C) for all stages.

Immunocytochemistry

Larvae were dissected on Sylgard plates in 1x PBST (0.3% Tween 20 [Fisher Scientific, BP337-500] in 1x phosphate-buffered saline [Gibco, 10010–023]). Dissected larvae were fixed by treating with 4% paraformaldehyde (Electron Microscopy Sciences, 50-980-487) for 10 min at room temperature (RT). Fixed larvae were washed three times with PBST for 10 min each time, then blocked by treating the larval samples with 1% bovine serum albumin (BSA; MP-Biomedicals, 0218062080) for 30 min. Samples were incubated with primary antibodies overnight at 4˚C followed by three washes with PBST for 10 min each time. Samples were then incubated overnight at 4˚C with secondary antibody, followed by three washes with PBST. Lastly, samples were mounted on slides using Vectashield containing DAPI (Vector laboratories, H-1200-10).

Mouse anti-polyubiquitin antibody (1:1000, EMD Millipore, ST1200-100UG) and rabbit anti-ref(2)P antibody (Srivastav et al., 2023) were the primary antibodies used in this work. The following secondary antibodies were used in this work: goat anti-mouse IgG coupled with FITC (1:1000, Abcam, ab6785) and donkey anti-rabbit IgG coupled to Alexa-fluor-647 (1:1000, Abcam, ab150075).

Neuromuscular junctions were immunostained with Alexa Fluor 647 conjugated rabbit anti-horseradish peroxidase (HRP; 1:1000, Jackson ImmunoResearch Laboratories, 323–605), an antibody that specifically recognizes the HRP epitope present on the surface of all Drosophila neurons.

Image quantitative analysis

Maximum intensity Z projections were obtained from 1 μm optical sections taken from the muscle apical surface until the entire muscle was imaged. All fluorescent images acquired were quantified and analyzed using the Surface module of Imaris v10.1. (Bitplane, Zurich, Switzerland) as previously described [13]. Poly-UB puncta number was obtained from the statistical data available for the surface created. The quantification of cytoplasmic poly-UB required an initial step in which nuclei were masked based on DAPI staining to remove inconsistent nuclear poly-UB signal.

Construction of flies bearing *Aop-atl*$^+$ and *Aop-atl*^{K51A}

The wildtype Drosophila *atlastin* coding sequence was generated by PCR from pJM681 [26], cut with NotI and XbaI, and ligated into pJFRC19-*13XlexAop2* (Addgene 26224), which contains 13 copies of the DNA binding sequence recognized by the LexA transcription factor (*Aop2*), to generate pJM1181. The coding sequence for the GTPase mutant atl^{K51A} was generated by PCR from pJM69 [26], cut with NotI and XbaI, and ligated into pJRC19 (Addgene 26224) to generate pJM1184. These constructs were introduced into embryos at the *attP2* site using with ϕC31-mediated recombination (GenetiVision, Houston TX). Insert-containing flies were recognized by eye color.

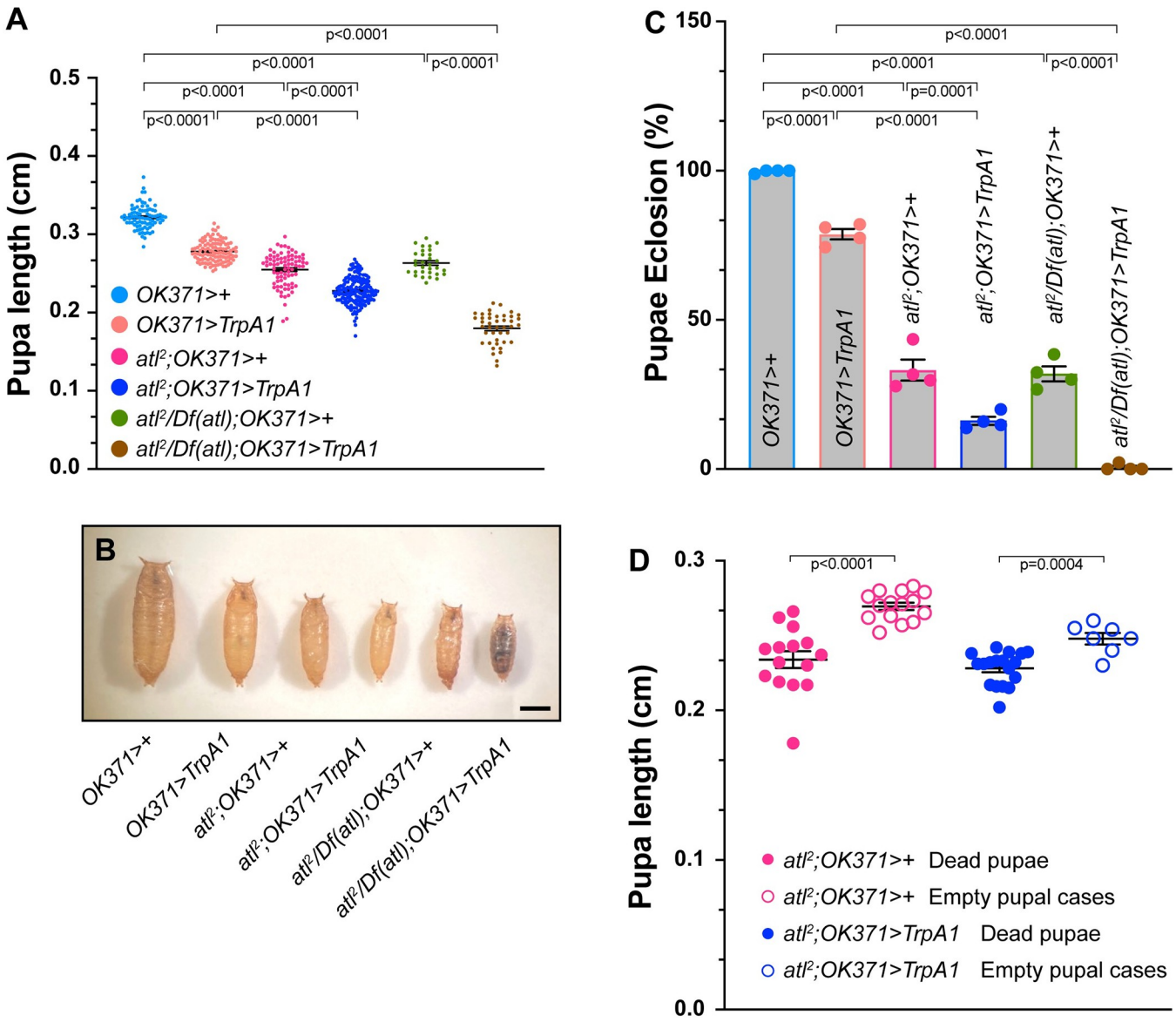

Fig 1. Enhancement of *atl*^{2} growth and viability phenotypes by TrpA1 activation. A) Pupal length (Y axis) from the indicated genotypes (color-coded, shown on X-axis) was measured with a dissecting stereomicroscope. Pupal length shown as a scatterplot. Means indicated by horizontal lines. n = 31–162. B) Representative images of pupae from the indicated genotypes (color-coded). Scale bar = 0.1 cm. C) Eclosion frequency (Y axis) of pupae from the indicated genotypes (X axis). Means+/- SEMS are shown. Genotypes were color-coded as in panel A and B. Each data point represents an independent experimental trial containing 30 pupae. n = 4. D) Lengths of empty pupal cases (open circles) and pupae containing dead animals (closed circles) of the indicated genotypes, shown as a scatterplot. Means +/- SEMs are indicated. n = 7–18. One-way ANOVA and Tukey's post-hoc test was used for statistical analysis shown in panels A and C. Student's t-test was used for statistical analysis shown in panel D.

https://doi.org/10.1371/journal.pone.0291477.g001

Antibody production and Western blotting

Recombinant Drosophila atlastin (soluble domain, amino acids 1–422, pJM781 [27]) was expressed in *E. coli* and purified by nickel affinity chromatography and used as an antigen to produce rabbit polyclonal antibodies (RC77, RC78, Cocalico Biologicals).

To measure Atlastin levels by Western blotting, protein extracts were generated either from whole flies (for *atl*^{2} and control) or heads (for *atlRNAi*, *atl*^{K51A} and controls). Following protein extraction, proteins were quantified, size-separated by SDS-PAGE chromatography, and

Western blotting was performed as described previously [13]. After transfer, membranes were blocked by treatment for 30 minutes with 5% powdered milk prepared in 1xTBST. Membranes were then incubated overnight at 4˚C with primary antibodies, followed by three washes in TBST for 10 minutes each. Membranes were then incubated with HRP-conjugated secondary antibodies for 2 hours at RT with mild shaking, followed by three washes in TBST for 10 minutes each. Membranes were then incubated with ECL reagent and observed in a LAS 4000 gel imager (Fujifilm). The following primary antibodies were used: rabbit anti-Atlastin polyclonal antibody (1:1000, RC78), and mouse anti-*Drosophila* β-tubulin antibody (1:1000, E7, DSHB). The secondary antibodies used were HRP-conjugated goat anti-mouse antibody (1:5000, #610–1319, Rockland), and HRP conjugated goat anti-Rabbit IgG (H+L) antibody (1:5000, Invitrogen, 31460).

Pupal length measurements

Pupal images were acquired with an Olympus trinocular microscope. ImageJ (National institutes of Health) was used to measure lengths along the central axis beginning with the anterior end.

Graphing and statistical analysis

All data analyzed in the present study were plotted and statistically analyzed using GraphPad Prism v9.3.1. One-way ANOVA with Tukey post-hoc analysis was used for all statistical analysis presented except for Fig 1D, for which Student's t-test was used.

Results

Enhancement of *atl*^{2} muscle phenotypes by motor neuron TrpA1 activation

Several lines of evidence suggest a link between neuronal excitability and neurodegeneration, but the mechanisms linking these processes remain incompletely understood. We addressed this question by examining effects of increasing neuronal excitability on Drosophila lacking the ER fusion/GTPase protein Atlastin *(*Atl*)* [26], which accumulate undegraded autophagic cargo and ubiquitinated protein aggregates (poly-UB aggregates) in larval muscle [13], and exhibit precocious degeneration of adult muscle [12]. We increased excitability in larval motor neurons by driving expression of *TrpA1*, which encodes a heat-inducible cation channel, with the *OK371* motor neuron *Gal4* driver, in which *Gal4* is inserted into the motor neuron-specific gene encoding the vesicular glutamate transporter, and rearing larvae at the elevated temperature of 28˚C. This protocol has been previously shown to increase neuronal excitability in larval motor neuron [28].

Larvae, pupae or adults lacking *atl* specifically in muscle exhibit a dwarf phenotype [13, 29, 30]. We determined whether TrpA1 activation affected body size in either a wildtype or *atl*^{2} background by measuring pupal length. Consistent with previous reports, we found that body size was significantly decreased in either *atl*^{2} or *atl/Df(atl)* pupae (Fig 1A, 1B). Furthermore, activating TrpA1 in motor neurons even in a wildtype background also significantly decreased pupal size. However, activating TrpA1 in an *atl*^{2} or *atl*^{2}*/Df(atl)* pupae decreased size significantly more than in *atl*^{2}, *atl*^{2}*/Df(atl)* or *TrpA1*-expressing pupae alone (Fig 1A, 1B). These results suggest that neuronal excitability enhances the *atl*^{2} dwarf phenotype, which is one phenotype conferred by *atl* loss in the muscle.

We found that TrpA1 activation likewise enhanced the defect in pupal eclosion conferred by *atl* loss. Whereas virtually all wildtype pupae are able to eclose to adults (Fig 1C), only about 30% of *atl*^{2} or *atl*^{2}*/Df(atl)* pupae are able do so. TrpA1 activation in otherwise wildtype pupae

also decreases eclosion frequency to ~75% successful eclosion. However, activating TrpA1 in pupae lacking *atl* decreases successful eclosion even further–to about 15% in atl^2 pupae, and to <1% in $atl^2/Df(atl)$ pupae (Fig 1C).

We found that the decreased ability to eclose conferred by atl^2 was strongly correlated with decreased pupal size. In Fig 1D, we compared sizes of pupae in which eclosion successfully occurred (empty pupal case) with pupal sizes in which eclosion failed (dead pupae). We found that empty pupal cases were significantly larger than cases containing dead pupae in atl^2 regardless of TrpA1 activation status. Thus, there is a positive correlation between eclosion frequency and pupal size, which is consistent with the possibility that TrpA1 activation decreases eclosion frequency in atl^2 because TrpA1 activation further decreases pupal size in atl^2.

In addition to decreased body size, larvae or adults lacking *atl* accumulate poly-UB aggregates within the muscle cytoplasm [12, 13]. To determine if TrpA1 activation would enhance the poly-UB phenotype conferred by *atl* loss, we examined effects of TrpA1 activation in muscle from wildtype, atl^2 and $atl^2/Df(atl)$ larvae. We found that TrpA1 activation in an otherwise wildtype background did not significantly increase cytoplasmic poly-UB aggregate number (Fig 2A, 2B and 2G). Cytoplasmic poly-UB aggregate number was not significantly affected in atl^2, whereas $atl^2/Df(atl)$ conferred a modest (p = 0.03) increase in aggregate number (Fig 2C, 2E and 2G). However, when TrpA1 activation was combined with either atl^2 or $atl^2/Df(atl)$,

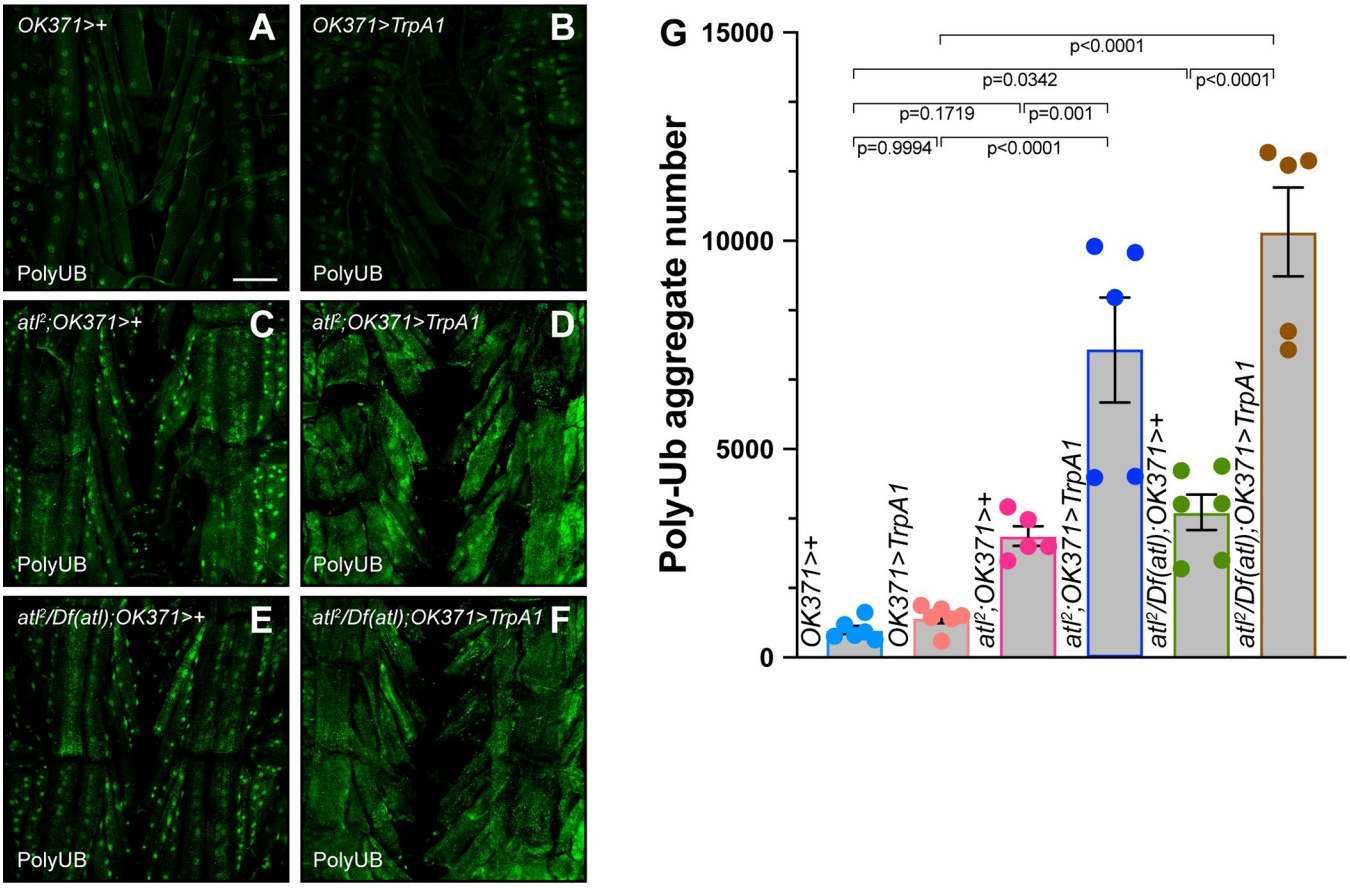

Fig 2. Enhancement of atl^2 poly-UB aggregate phenotype by TrpA1 activation. A)-F) Confocal imaging (maximum intensity z projection) of fixed third instar larval musculature from muscle 6 stained with an anti-ubiquitin antibody (green). Scale bar = 100 μm. G) Means +/- SEMs of cytoplasmic poly-UB aggregate number (Y axis) as a function of genotype (X axis). Genotypes were color coded as shown in Fig 1A and 1B. Ubiquitin from nuclei, identified from the DAPI channel, was removed prior to quantification. One-way ANOVA and Tukey's post-hoc test was used for statistical analysis. n = 5–6.

https://doi.org/10.1371/journal.pone.0291477.g002

poly-UB aggregate number was significantly increased over atl^2, $atl^2/Df(atl)$ or *TrpA1*-expressing larvae alone (Fig 2D, 2F and 2G). Thus, TrpA1 enhances the larval muscle poly-UB phenotype conferred by *atl* loss.

The increased number of poly-UB aggregates conferred by TrpA1 activation in an *atl* null background raised the possiblity TrpA1 activation was enhancing an autophagy deficit conferred by *atl* null larvae. To confirm this possibility, we determined if these poly-UB-containing punctae also contained the autophagy receptor ref(2)P (also known as p62 or SQSTM1). We found that TrpA1 activation did not significantly increase ref(2)P aggregate number in an otherwise wildtype background, but significantly increased number of these aggregates in atl^2 (S1A–S1M Fig). Furthermore, TrpA1 activation in an atl^2 background did not affect the extent of colocalization between poly-UB and ref(2)P (S2 Fig). These results indicate that the additional poly-UB aggregates generated as a consequence of TrpA1 activation were intermediates of the autophagy pathway.

TrpA1 activation does not enhance phenotypes conferred by neuronal *atl* loss

Various muscle properties are affected by *atl* loss specifically in cell autonomous processes in the muscle, whereas others are affected by *atl* loss specifically in synaptically-driven processes in motor neurons. For example, muscle *atl* loss increases the number of poly-UB-containing protein aggregates in both adult and larval muscle [12, 13]. *atl* loss specifically from neurons likewise increases the number of poly-UB-containing aggregates in adult muscle, but effects on larval muscle aggregate number have not been reported. Similarly, muscle *atl* loss is sufficient to decrease body size [13], but effects of neuronal *atl* loss on body size have not been reported. The enhancement by TrpA1 activation of the body size and poly-UB phenotypes conferred by atl^2 could reflect loss of *atl* from either neuron or muscle. To determine if *atl* loss in neurons was responsible for enhancement by TrpA1 activation, we used RNAi to knockdown *atl* specifically in motor neurons and determined if TrpA1 activation was still capable of enhancing phenotypes of *atl* loss.

First, we examined effects of neuronal *atl* knockdown and TrpA1 activation on body size and eclosion frequency, using the motor neuron *Gal4* driver *OK371* to express both the *atl RNAi* construct and *TrpA1*. We found, consistent with what we showed in Fig 1 above, that TrpA1 activation significantly decreased pupal size (Fig 3A and 3B). However, *atl* knockdown in motor neurons had no effect on pupal size (Fig 3A and 3B), and TrpA1 activation only slightly decreased size in *atl* knockdown pupae. These results indicate that *atl* loss in neurons is not sufficient to decrease body size and that TrpA1 activation does not interact with neuronal *atl* loss to control body size.

Neuronal *atl* loss is likewise not sufficient to decrease pupal eclosion frequency, either in the presence or absence of TrpA1 activation (Fig 3C). Furthermore, whereas TrpA1 activation in an otherwise wildtype background decreased pupal eclosion frequency, consistent with what was shown in Fig 1, TrpA1 activation failed to decrease eclosion frequency in the context of neuronal *atl* knockdown. In fact, neuronal *atl* knockdown unexpectedly appeared to rescue the effects of TrpA1 activation on eclosion frequency, an observation that we attribute to the presence of three *UAS*-driven transgenes in these pupae, which together titrate limiting Gal4 and consequently decrease the amount of *UAS*-driven expression from these transgenes.

Second, we examined effects of neuronal *atl* loss and TrpA1 activation on muscle poly-UB aggregate accumulation. As shown in Fig 4, TrpA1 activation in an otherwise wildtype background did not significantly affect muscle poly-UB aggregate accumulation (Fig 4A, 4B and 4E). In contrast, neuronal *atl* knockdown increased poly-UB aggregate number significantly,

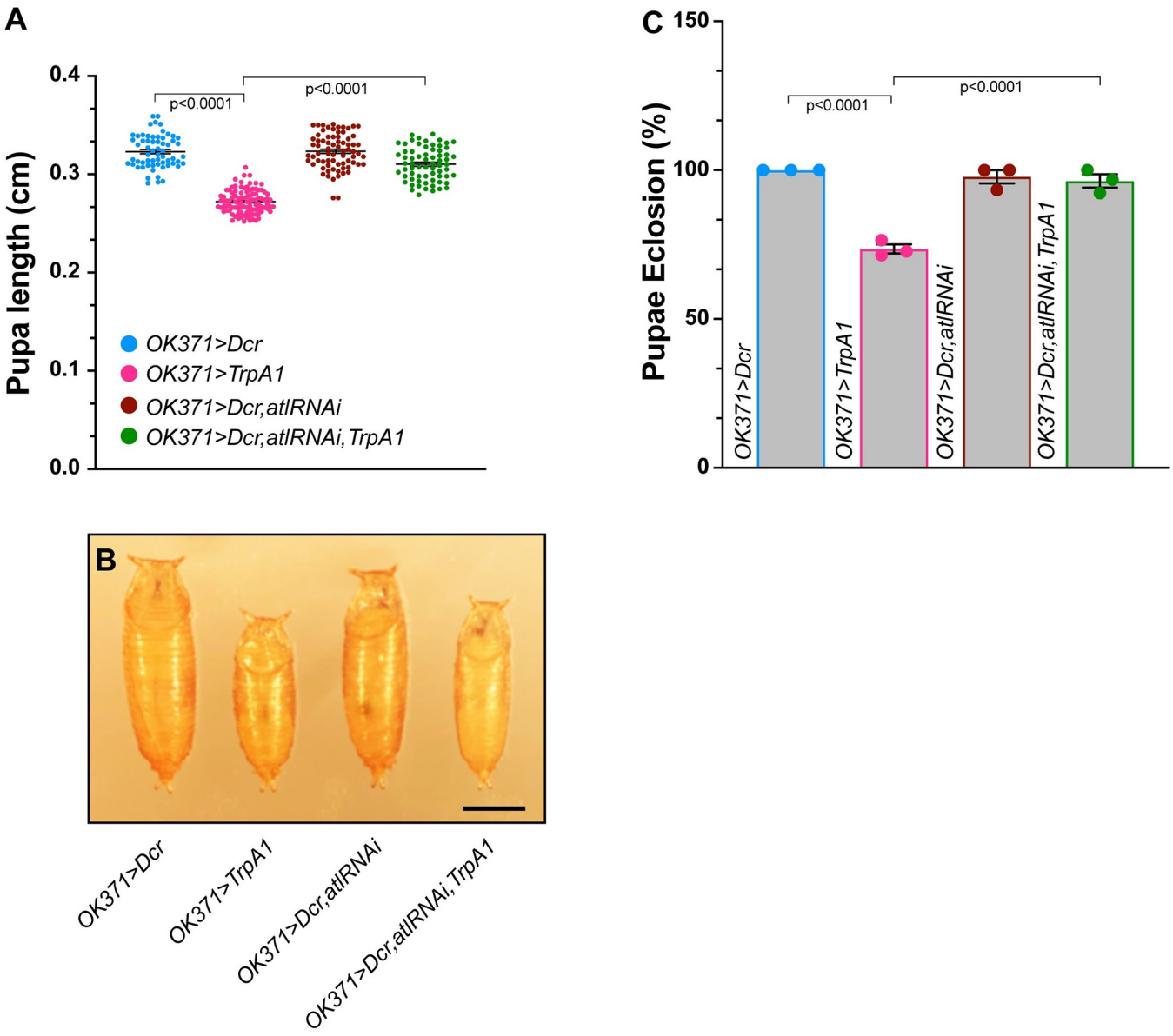

Fig 3. Neuronal *atl* knockdown fails to enhance the growth and viability phenotypes of TrpA1 activation. A) Pupal length (Y axis) from the indicated genotypes (color-coded, shown on X-axis) was measured with a dissecting stereomicroscope. Pupal length shown as a scatterplot. Means indicated by horizontal lines. n = 62–101. B) Representative images of pupae from the indicated genotypes (color-coded). Scale bar = 0.1 cm. C) Eclosion frequency (Y axis) of pupae from the indicated genotypes (X axis). Means+/- SEMS are shown. Genotypes were color-coded as in panel A and B. n = 3.

https://doi.org/10.1371/journal.pone.0291477.g003

albeit modestly (Fig 4C and 4E), which demonstrates that neuronal *atl* loss increases poly-UB aggregate number in larval as well as adult muscle, consistent with previous reports [12]. However, we found no further increase in muscle poly-UB aggregate number when we activated TrpA1 in a background of neuronal *atl* knockdown (Fig 4D and 4E). Taken together, these results demonstrate that *TrpA1* does not enhance phenotypes conferred by neuronal *atl* loss.

TrpA1 activation enhances phenotypes conferred by muscle *atl* loss

The observation that TrpA1 activation enhanced muscle phenotypes of atl^2 but not neuronal *atl* knockdown raised the possibility that this enhancement required *atl* loss from muscle. To

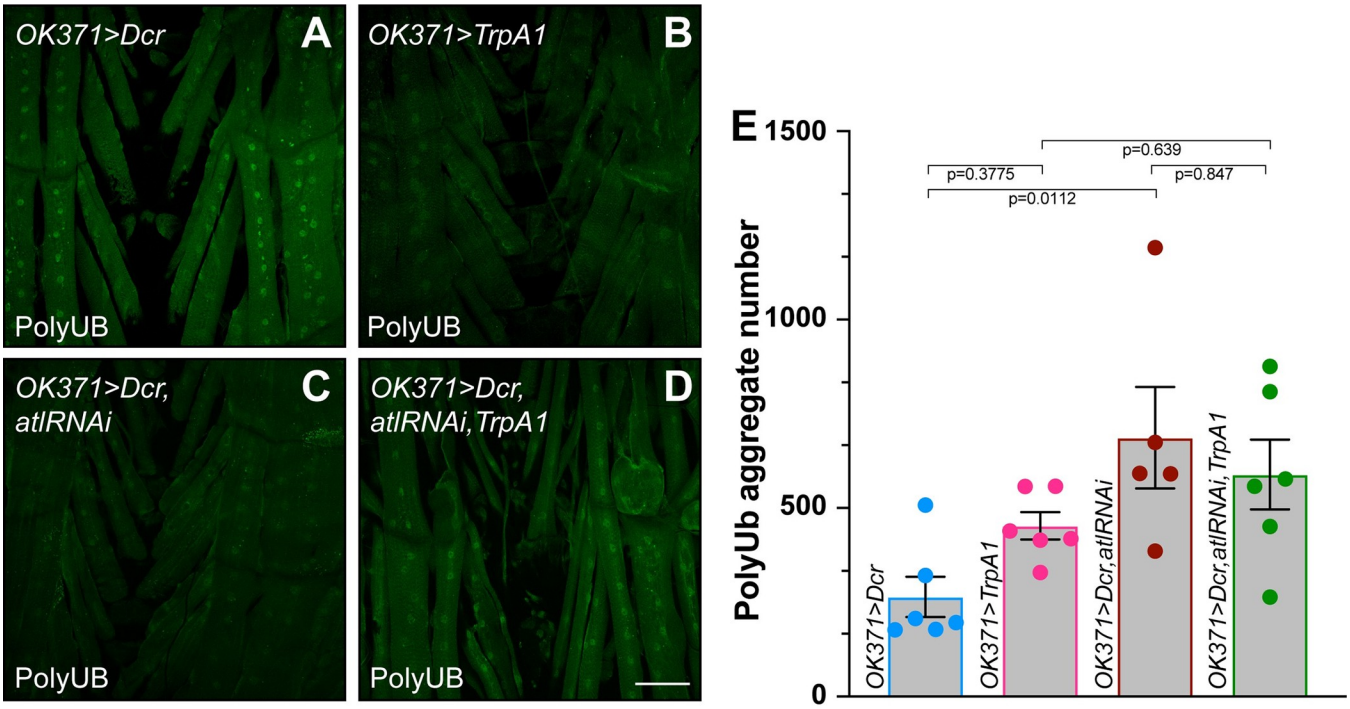

Fig 4. TrpA1 activation fails to enhance poly-UB aggregate accumulation conferred by neuronal *atl* knockdown. A)-D) Confocal imaging (maximum intensity z projection) of fixed third instar larval musculature from muscle 6 stained with an anti-ubiquitin antibody (green). Scale bar = 100 μm. E) Means +/- SEMs of cytoplasmic poly-UB aggregate number (Y axis) as a function of genotype (X axis). Genotypes were color coded as shown in Fig 3A. Ubiquitin from nuclei, identified from the DAPI channel, was removed prior to quantification. One-way ANOVA and Tukey's post-hoc test was used for statistical analysis. n = 5–6.

https://doi.org/10.1371/journal.pone.0291477.g004

test this possibility, we needed to independently activate TrpA1 in neurons while knocking down *atl* in muscle. To accomplish this goal, we used the *nSyb-LexA* panneuronal driver from the LexA/Aop system [31] to drive expression of *Aop*-driven *TrpA1* [32, 33]. We simultaneously used the *24B* muscle Gal4 driver to drive expression of *UAS*-driven *atl* RNAi construct, as performed previously [13].

We used two tests to validate *nSyb-LexA* as a driver capable of expressing *TrpA1* sufficiently to confer a neuronal excitability phenotype. First, we generated an antibody against Drosophila Atlastin expressed as a recombinant protein from *E. coli*. This antibody specifically recognizes Drosophila Atlastin, as the atl^2 deletion mutation eliminates the major band observed at 50 kd (S2A Fig). We used this antibody to compare Atlastin protein levels from heads in which either of two, *Aop*-driven constructs were expressed under the control of *nSyb-LexA*: first, an *atl* coding construct carrying the dominant-negative atl^{K51A} allele, and second, an *atl* RNAi construct [25]. We found that *nSyb-LexA* driving atl^{K51A} increased head Atlastin protein levels approximately 7-fold over heads from *nSyb-LexA* driving the parent empty *attP2* site (S2B Fig). Similarly, we found that *nSyb-LexA* driving *atlRNAi* decreased head Atlastin protein levels 4-fold over heads from *nSyb-LexA* driving the parent empty *attP2* site (S2C Fig). These results validate *nSyb-LexA* as an effective driver of *Aop*-driven transgenes in neurons. Note that *nSyb-LexA* driving *Aop-*atl^+ was lethal at the embryonic stage, consistent with the previous report that *elav-Gal4*-driven atl^+ is embryonic lethal [24]. Second, we examined behavior of flies bearing both *nSyb-LexA* and *Aop-TrpA1* and found that etherized adults under fiber optic illumination displayed vigorous leg shaking, a hallmark of adults with increased neuronal excitability [34]. This leg shaking was similar to the leg shaking displayed by flies bearing both

OK371 and *UAS-TrpA1* but was absent from *nSyb-LexA* adults that did not carry *Aop-TrpA1*. Taken together, these observations confirm that *nSyb-lexA* driver effectively drives expression of *Aop*-driven transgenes within neurons.

We found that activating TrpA1 with the LexA/Aop system significantly decreased pupal size to an extent similar to the decrease found when TrpA1 was activated with the Gal4 system (Fig 5A and 5B). Furthermore, as described previously [13], we found that knocking down *atl* specifically in muscle also decreased pupal size. However, in contrast to the lack of enhancement when *atl* was knocked down in motor neurons, *atl* knockdown in muscle significantly

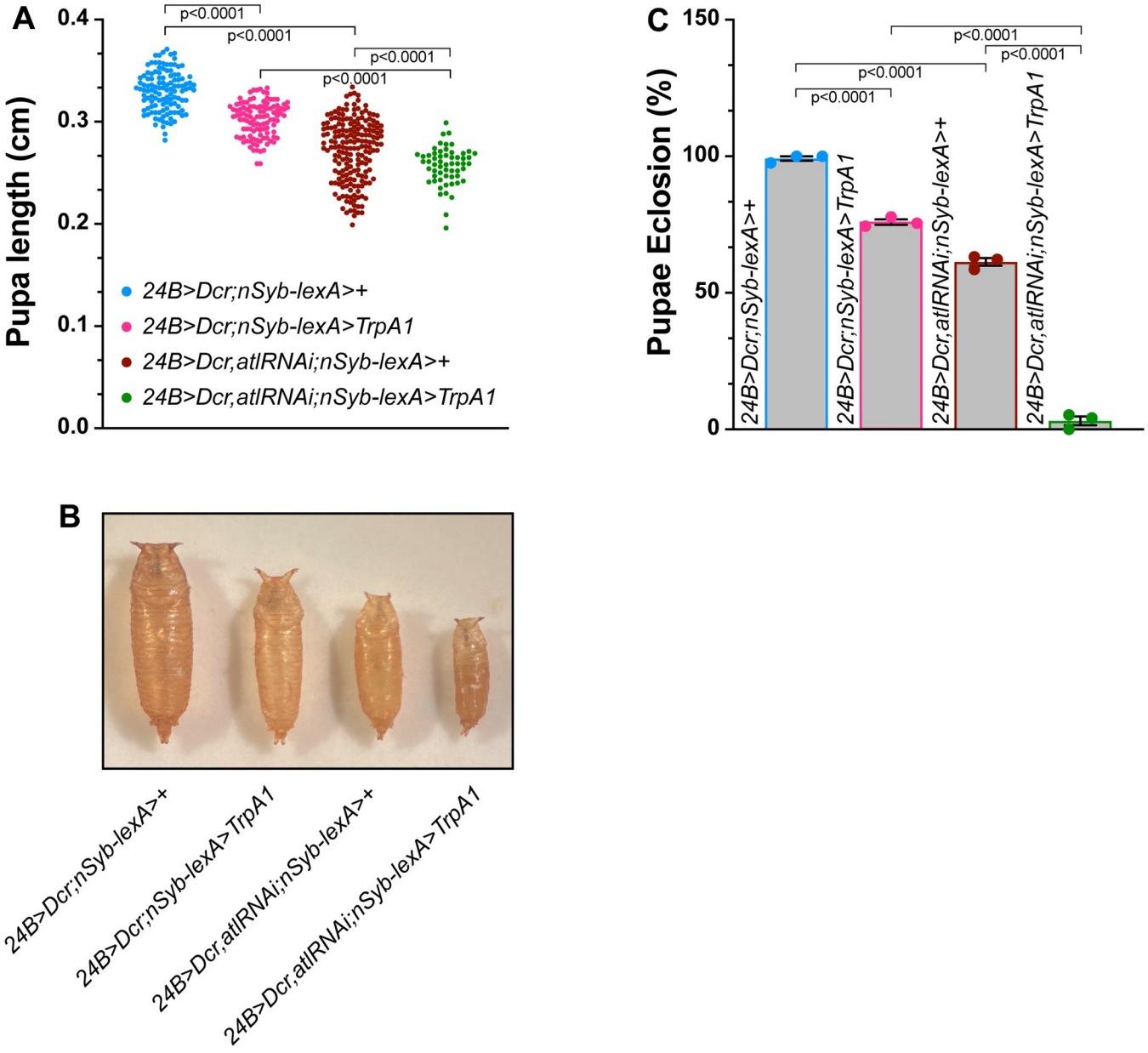

Fig 5. TrpA1 activation enhances the growth and viability deficits of muscle *atl* knockdown. A) Pupal length (Y axis) from the indicated genotypes (color-coded, shown on X-axis) was measured with a dissecting stereomicroscope. Pupal length shown as a scatterplot. Means indicated by horizontal lines. n = 58–190. B) Representative images of pupae from the indicated genotypes (color-coded). Scale bar = 0.1 cm. C) Eclosion frequency (Y axis) of pupae from the indicated genotypes (X axis). Means+/- SEMS are shown. Genotypes were color-coded as in panel A. n = 3.

https://doi.org/10.1371/journal.pone.0291477.g005

enhanced the effects of TrpA1 activation on pupal size (Fig 5A and 5B). We conclude that the enhancement of the *atl* body size phenotype by TrpA1 activation requires *atl* loss in muscle but not neurons.

We also examined the effect of TrpA1 activation on eclosion frequency in muscle *atl* knockdown pupae. We found that control pupae exhibited an almost 100% frequency of eclosion (Fig 5C), consistent with what we observed for the control pupae described above. Furthermore, activating TrpA1 in an otherwise wildtype background significantly decreased pupal eclosion frequency to about 75% (Fig 5C), an observation also consistent with what we found for *Gal4*-driven *TrpA1* expression described above. Similarly, muscle *atl* knockdown in the absence of *TrpA1* expression significantly decreased eclosion frequency to about 60% (Fig 5B). However, activating TrpA1 in pupae with muscle lacking *atl* decreased successful eclosion to only about 2%. We conclude that the enhancement of the *atl* eclosion phenotype by TrpA1 activation requires *atl* loss in muscle but not neurons.

As described above, TrpA1 activation enhanced the increase in muscle poly-UB aggregate number conferred by atl^2 but not neuronal *atl* loss. To determine if TrpA1 activation would enhance the poly-UB phenotype conferred by muscle *atl* loss, we compared effects of TrpA1 activation on cytoplasmic poly-UB from wildtype and *atl* knockdown muscle (Fig 6). We found that TrpA1 activation in an otherwise wildtype background did not significantly increase cytoplasmic poly-UB aggregate number (Fig 6A, 6B and 6E), consistent with observations described above. Muscle *atl* knockdown in the absence of TrpA1 activity significantly increased cytoplasmic poly-UB aggregate number, consistent with previous reports (Fig 6C and 6E) [13]. When we combined TrpA1 activation with muscle *atl* knockdown, poly-UB aggregate number was significantly increased compared to either muscle *atl* knockdown or

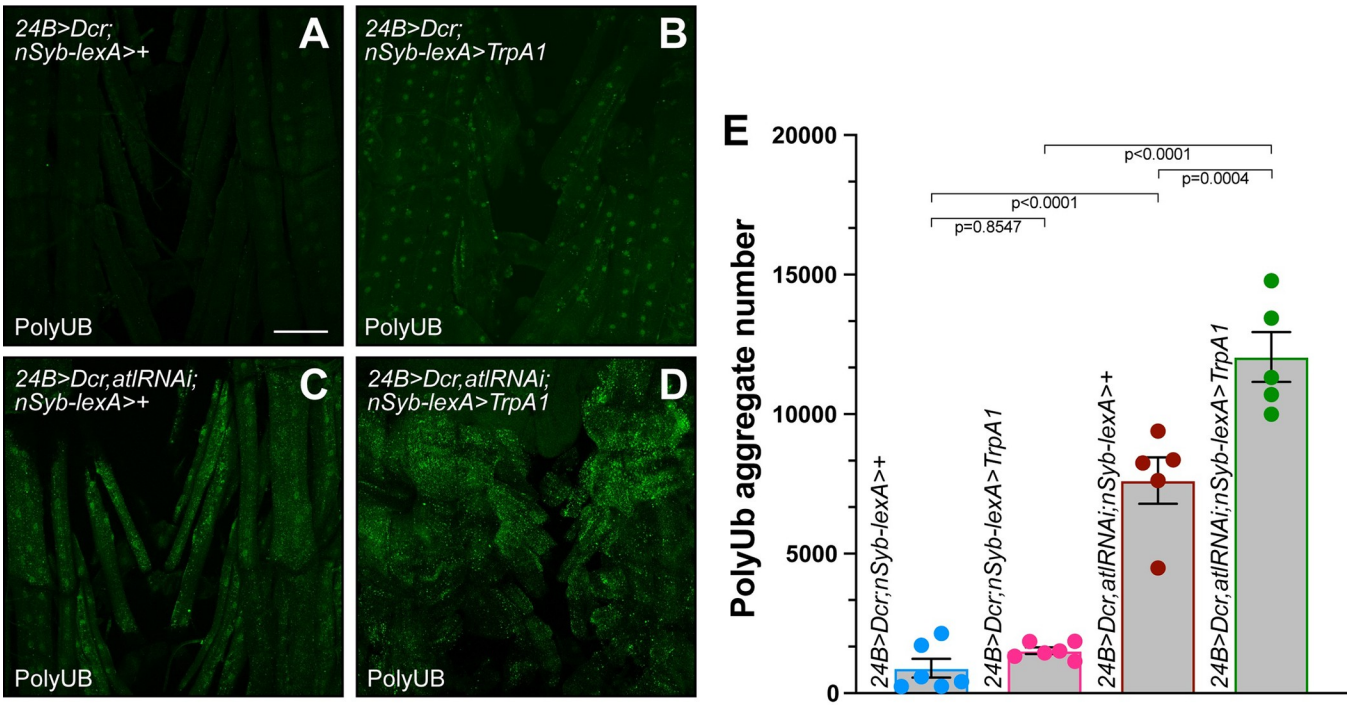

Fig 6. TrpA1 activation enhances the effects of muscle *atl* knockdown on poly-UB aggregate accumulation. A)-D) Confocal imaging (maximum intensity z projection) of fixed third instar larval musculature from muscle 6 stained with an anti-ubiquitin antibody (green). Scale bar = 100 μm. E) Means +/- SEMs of cytoplasmic poly-UB aggregate number (Y axis) as a function of genotype (X axis). Genotypes were color coded as shown in Fig 5A. Ubiquitin from nuclei, identified from the DAPI channel, was removed prior to quantification. One-way ANOVA and Tukey's post-hoc test was used for statistical analysis. n = 5–6.

https://doi.org/10.1371/journal.pone.0291477.g006

TrpA1 activation (Fig 6D and 6E). Thus, TrpA1 activation significantly enhances the larval muscle poly-UB phenotype conferred by muscle, but not neuronal, *atl* loss.

TrpA1 activation fails to enhance *atl* effects on axon branching and synaptic bouton number

Loss of *atl* from either neurons or muscle confers penotypes in addition to muscle poly-UB aggregate accumulation and body size defects. For example, *atl* loss from either neurons or muscle increases axon branch and synaptic bouton number at the larval neuromuscular junction (NMJ) [13, 24]. We tested if these NMJ phenotypes could be altered by TrpA1 activation in a manner similar to the poly-UB and body size deficits. We found that neuronal *atl* knockdown significantly increased both axon branch and synaptic bouton number (S3D Fig), consistent with previous report [24]. However, TrpA1 activation had no effect on these NMJ phenotypes in a neuronal *atl* knockdown background (S3 Fig). Likewise, the increased synaptic branch and bouton number conferred by muscle *atl* knockdown was not further enhanced by TrpA1 activation (S3 Fig). We conclude that only certain phenotypes of *atl* loss are enhanced by increased neuronal excitability.

Enhancement of atl^2 poly-UB phenotypes by a second excitability transgene

To determine if the interactions between TrpA1 activation and muscle *atl* loss on poly-UB aggregate accumulation was specific to TrpA1, or could be observed with other excitability transgenes, we tested if expressing a second excitability transgene would likewise enhance the cytoplasmic poly-UB phenotype of atl^2. We chose a transgene carrying a dominant-negative mutation in *Shaker (Sh)*, which encodes a potassium channel subunit. We chose this transgene because its effects on excitability are particularly well documented [35–38]. We found that *OK371*-driven Sh^{DN} expression in an otherwise wildtype background had no effect on larval muscle poly-UB aggregate number (Fig 7A, 7B and 7E). In contrast, this expression of Sh^{DN} significantly enhanced the effects of atl^2 on aggregate number (Fig 7C, 7D and 7E).

Discussion

Several lines of evidence demonstrate a link between conditions that increase neuronal excitability and proteomic stress [16, 39, 40]. However, neither the causal relationship between these phenomena nor the mechanisms underlying this linkage are completely understood. Here we use the glutamatergic Drosophila larval neuromuscular junction to address these questions. We increased neuronal excitability by activating the TrpA1 cation channel in motor neurons and induced proteomic stress in larval muscle by inhibiting ER fusion and disrupting autophagy by deletion of *atlastin* [12, 13]. We found that TrpA1 activation enhanced several phenotypes conferred by the null atl^2 mutation. Most notably, TrpA1 activation enhanced the atl^2-dependent accumulation of muscle cytoplasmic aggregates containing ubiquitin (poly-UB aggregates). We combined the *Gal4* and *LexA* transgene expression systems to determine that *atl* loss in muscle but not neuron was responsible for this enhancement. Expressing a second excitability transgene, a dominant-negative mutation in the *Shaker (Sh)*-encoded potassium channel (Sh^{DN}), within motor neurons likewise enhanced the poly-UB aggregate accumulation phenotype of atl^2. These results suggest that increasing neuronal activity presynaptically can induce proteomic stress in the postsynaptic cell, which can be revealed in the background of certain neurodegeneration mutants. These studies thus provide one potential mechanism for mechanistic linkage between neuronal excitability and neurodegeneration.

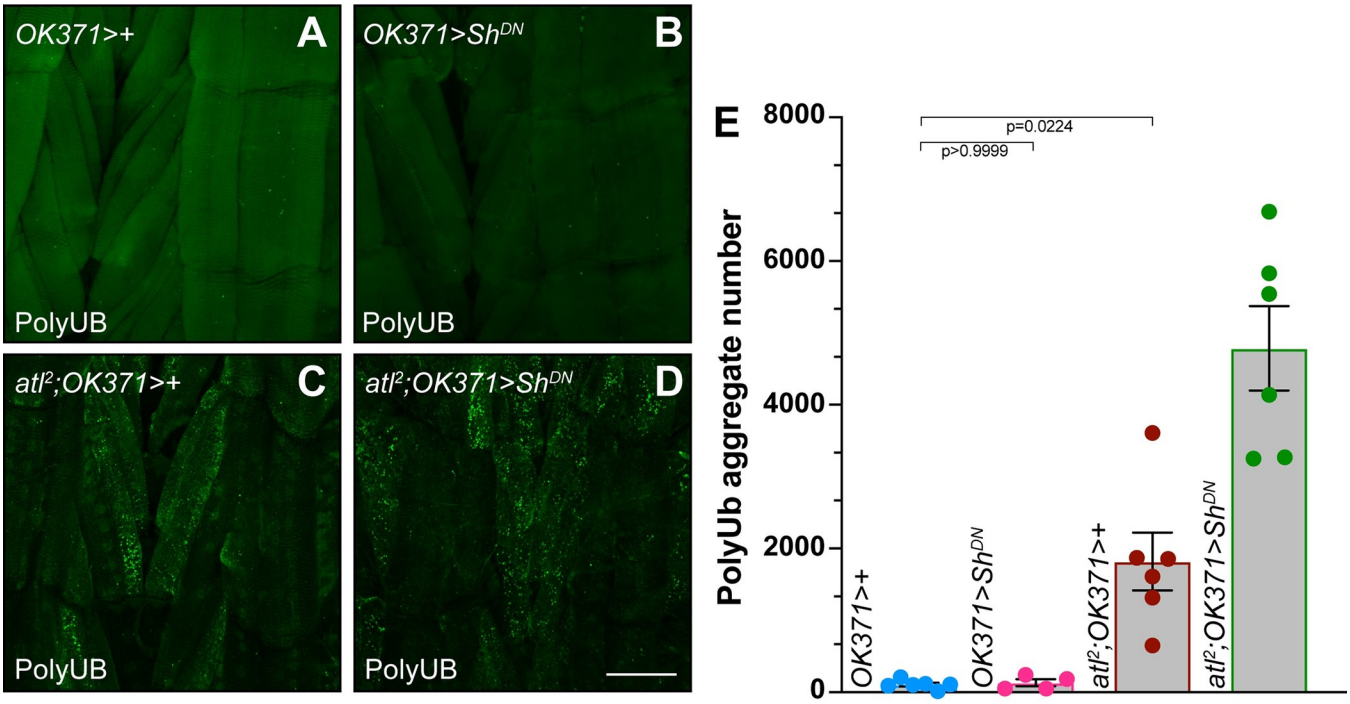

Fig 7. Enhancement of the *atl*^{2} poly-UB aggregate accumulation phenotype by *Sh*^{DN} expression. A)-D) Confocal imaging (maximum intensity z projection) of fixed third instar larval musculature from muscle 6 stained with an anti-ubiquitin antibody (green). Scale bar = 100 μm. E) Means +/- SEMs of cytoplasmic poly-UB aggregate number (Y axis) as a function of genotype (X axis). Ubiquitin from nuclei, identified from the DAPI channel, was removed prior to quantification. One-way ANOVA and Tukey's post-hoc test was used for statistical analysis.

https://doi.org/10.1371/journal.pone.0291477.g007

How might motor neuron activity induce proteomic stress in muscle?

There are several possible mechanisms by which increased neuronal excitability could induce proteomic stress in the postsynaptic cell. Two non-mutually exclusive mechanisms include increasing muscle metabolic activity and hence mitochondrial reactive oxygen species (ROS) production or increasing muscle cytoplasmic [Ca^{2+}]. Increasing ROS production could accelerate formation of oxidatively damaged proteins and lead to increased production of cytoplasmic protein aggregates. Increasing cytoplasmic [Ca^{2+}] has been shown to induce various toxic processes, such as activating the Calpain protease [21], and has been implicated in neuronal death occurring as a consequence of glutamate toxicity [20, 22]. Indeed, various investigators have proposed Ca^{2+} toxicity as a potential contributor to neuronal death in various neurodegenerative disorders [41, 42]. These possibilities could be addressed in future studies.

Activity dependent proteomic stress in muscle revealed by loss of *atl*

Our data show that increasing neuronal excitability has little to no observable effect on muscle proteomic stress in an otherwise wildtype background, but significantly increases proteomic stress in the absence of *atl*. We suggest two possibilities to explain this synergistic interaction. First, increasing neuronal excitability increases protein damage in the target muscle, possibly as a consequence of increased ROS production as described above. In this view, the wildtype muscle has sufficient reserve capacity of autophagy machinery to handle this increase in protein damage without observable increases in poly-UB aggregate accumulation (Fig 8). In contrast, this reserve autophagy capacity is eliminated by *atl* loss, leading to an inability to handle the increased protein damage caused by neuronal activity. Consequently, these damaged

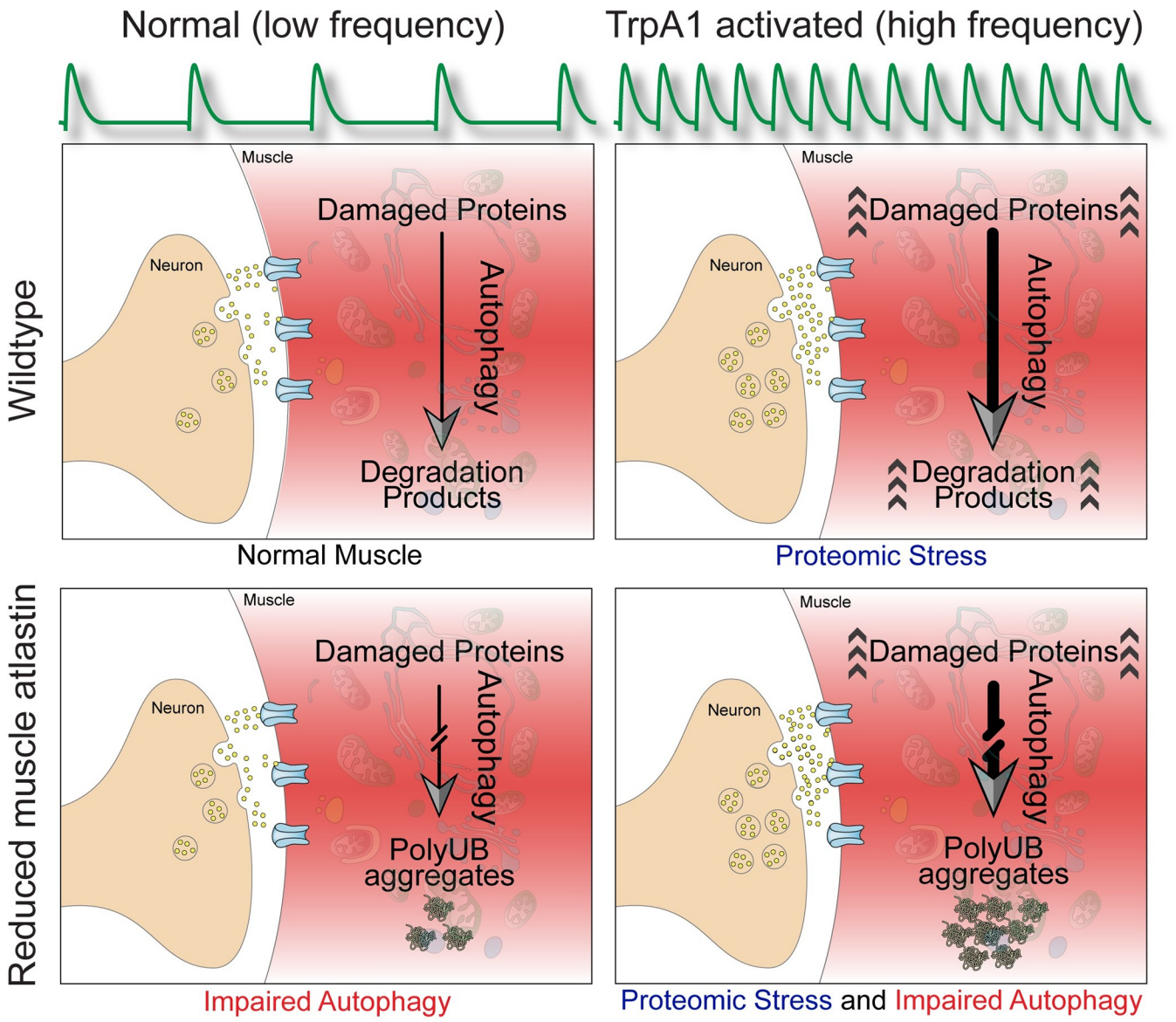

Fig 8. Enhancement of the *atl*^{2} poly-UB aggregate accumulation phenotype by increased neuronal excitability. At the wildtype neuromuscular junction (upper left panel), low frequency motor neuron action potentials (upper green trace) triggers fusion of synaptic vesicles (green circles) with the cell membrane, releasing neurotransmitter (l-glutamate, small green circles) into the synaptic cleft and enabling binding glutamate receptors (blue) on the surface of the muscle (pink). Damaged proteins are degraded via the autophagy pathway. In muscle lacking *atl* (lower left panel), the autophagy pathway is attenuated, leading to accumulation of protein aggregates. TrpA1 activation (right panels) increases motor neuron action potential frequency, leading to increased release of neurotransmitter and increase in protein damage (arrowheads). Whereas the *atl*$^{+}$ muscle can increase autophagy to accommodate this increased protein damage (upper right panel), the attenuated autophagy in muscle lacking *atl* (lower right panel) prevents this accommodation and leads to increased accumulation of protein aggregates.

https://doi.org/10.1371/journal.pone.0291477.g008

proteins accumulate as poly-UB containing aggregates (Fig 8). Second, neuronal activity partially inhibits autophagy in the target muscle. Whereas the wildtype muscle has sufficient reserve capacity of autophagy machinery to handle this inhibition without difficulty, *atl* loss eliminates this reserve capacity and sensitizes the muscle to the further crippling of autophagy caused by increased neuronal excitability, leading to the observed enhancement of poly-UB aggregate accumulation.

Relevance to neurodegenerative disorders

This work describes excitability-driven enhancement of proteomic stress specifically at the neuromuscular junction. Extrapolating these interactions to central synapses would afford relevance to other neurodegenerative disorders. In this view, neuronal activity would transition from benign to toxic as postsynaptic autophagy deficits begin and protein aggregates accumulate. Such a process could explain the well-established ability of conditions that increase excitability, such as epilepsy, to contribute to pathology of neurodegeneration. Furthermore, the observation that neurodegenerative processes can also feedback to increase neuronal excitability raises the possibility that neuronal excitability and neurodegeneration can together form a positive feedback loop, ultimately leading to exponential increases in both neuronal excitability and neurodegeneration. If so, then pharmacological interventions that depress neuronal excitability could sever this positive feedback and thus be beneficial in the treatment of a variety of neurodegenerative disorders.

Supporting information

S1 Fig. TrpA1 activation increases ref(2)P-containing aggregate accumulation in *atl* null larval muscle. A)-L) Confocal imaging (maximum intensity z projection) of fixed third instar larval muscle cell 6 of the indicated genotypes stained with an anti-ubiquitin antibody (green, panels A,D,G,J), an anti-ref(2)P antibody (red, panels B,E,H,K) and merge (panels C,F,I,L). Scale bar 20 μm. M) Means +/- SEMs of ref(2)P aggregate number (Y axis) as a function of genotype (X axis). N) Percent of the poly-UB punctae that are also contain ref(2)P (Y axis) for the indicated genotypes. P-values were calculated by Student's t-test. All larvae were reared at 28˚ C.
(TIF)

S2 Fig. Validation of *nSyb-lexA* driver for pan-neuronal induction of gene expression. A) Western blot with anti-Atl antibody from whole fly from wildtype (*attP2*, lanes 1 and 2), atl^{2} (lanes 3 and 4), and recombinant GST and His-tagged Atl (lanes 5 and 6). B) Heads from flies carrying *nSyb-lexA* and either *Aop*-driven atl^{K51A} (lanes 2 and 4) or empty vector (lanes 1 and 3). C) Heads from flies carrying *nSyb-lexA* and either empty vector (lanes 1 and 2) or *Aop*-driven *atl RNAi* (lanes 3 and 4). β-tubulin serves as loading control in B) and C).
(TIF)

S3 Fig. TrpA1 activation fails to enhance the increase in synaptic bouton number and axon branching conferred by *atl* loss. Larval nerves innervating muscles 6 and 7 were labelled with Alexa fluor 647 conjugated anti-HRP and imaged on a Zeiss LSM 800 with a 40x objective. A)-D) and G)-J) show neuromuscular junctions from larvae of the indicated genotypes, shown in pseudo cyan. E), F), K), and L) Scattergram showing means +/- SEMs of bouton number (E) and axon branch number (F) for larvae of genotypes. p values were calculated by a one-way ANOVA and Tukey's post-hoc test. n = 5 or 6.
(TIF)

S1 Raw images.
(PDF)

Acknowledgments

We are grateful to the Bloomington Drosophila Stock Center, Tim Mosca, Gerry Rubin and Kristin Scott for provided Drosophila stocks. This work conducted, in part, using resources of the Rice University Shared Equipment Authority.

Author Contributions

Conceptualization: Saurabh Srivastav, Kevin van der Graaf.

Formal analysis: Saurabh Srivastav, James A. McNew, Michael Stern.

Funding acquisition: James A. McNew, Michael Stern.

Investigation: Saurabh Srivastav, Kevin van der Graaf, Prisha C. Jonnalagadda, Maanvi Thawani.

Methodology: Saurabh Srivastav, Kevin van der Graaf.

Project administration: James A. McNew, Michael Stern.

Resources: James A. McNew.

Supervision: James A. McNew, Michael Stern.

Writing – original draft: Michael Stern.

Writing – review & editing: Saurabh Srivastav, James A. McNew, Michael Stern.

References

1. Hou X, Watzlawik JO, Fiesel FC, Springer W. Autophagy in Parkinson's Disease. J Mol Biol. 2020; 432 (8):2651–72. Epub 20200213. https://doi.org/10.1016/j.jmb.2020.01.037 PMID: 32061929.
2. Liu J, Li L. Targeting Autophagy for the Treatment of Alzheimer's Disease: Challenges and Opportunities. Front Mol Neurosci. 2019; 12:203. Epub 20190822. https://doi.org/10.3389/fnmol.2019.00203 PMID: 31507373.
3. Martin DD, Ladha S, Ehrnhoefer DE, Hayden MR. Autophagy in Huntington disease and huntingtin in autophagy. Trends Neurosci. 2015; 38(1):26–35. Epub 20141002. https://doi.org/10.1016/j.tins.2014.09.003 PMID: 25282404.
4. Komatsu M, Waguri S, Chiba T, Murata S, Iwata J, Tanida I, et al. Loss of autophagy in the central nervous system causes neurodegeneration in mice. Nature. 2006; 441(7095):880–4. https://doi.org/10.1038/nature04723 PMID: 16625205.
5. Komatsu M, Waguri S, Koike M, Sou YS, Ueno T, Hara T, et al. Homeostatic levels of p62 control cytoplasmic inclusion body formation in autophagy-deficient mice. Cell. 2007; 131(6):1149–63. https://doi.org/10.1016/j.cell.2007.10.035 PMID: 18083104.
6. Rubinsztein DC. The roles of intracellular protein-degradation pathways in neurodegeneration. Nature. 2006; 443(7113):780–6. https://doi.org/10.1038/nature05291 PMID: 17051204.
7. Williams A, Jahreiss L, Sarkar S, Saiki S, Menzies FM, Ravikumar B, et al. Aggregate-prone proteins are cleared from the cytosol by autophagy: therapeutic implications. Curr Top Dev Biol. 2006; 76:89–101. https://doi.org/10.1016/S0070-2153(06)76003-3 PMID: 17118264.
8. Clemen CS, Tangavelou K, Strucksberg KH, Just S, Gaertner L, Regus-Leidig H, et al. Strumpellin is a novel valosin-containing protein binding partner linking hereditary spastic paraplegia to protein aggregation diseases. Brain. 2010; 133(10):2920–41. Epub 20100909. https://doi.org/10.1093/brain/awq222 PMID: 20833645.
9. Khundadze M, Ribaudo F, Hussain A, Stahlberg H, Brocke-Ahmadinejad N, Franzka P, et al. Mouse models for hereditary spastic paraplegia uncover a role of PI4K2A in autophagic lysosome reformation. Autophagy. 2021; 17(11):3690–706. Epub 20210309. https://doi.org/10.1080/15548627.2021.1891848 PMID: 33618608.
10. Vantaggiato C, Crimella C, Airoldi G, Polishchuk R, Bonato S, Brighina E, et al. Defective autophagy in spastizin mutated patients with hereditary spastic paraparesis type 15. Brain. 2013; 136(Pt 10):3119–39. Epub 20130911. https://doi.org/10.1093/brain/awt227 PMID: 24030950.
11. Liu N, Zhao H, Zhao YG, Hu J, Zhang H. Atlastin 2/3 regulate ER targeting of the ULK1 complex to initiate autophagy. J Cell Biol. 2021; 220(7). Epub 20210514. https://doi.org/10.1083/jcb.202012091 PMID: 33988678.
12. Xu S, Stern M, McNew JA. Beneficial effects of rapamycin in a Drosophila model for hereditary spastic paraplegia. J Cell Sci. 2017; 130(2):453–65. https://doi.org/10.1242/jcs.196741 PMID: 27909242.

13. Srivastav S, van der Graaf K, Singh P, Utama AB, Meyer MD, McNew JA, et al. atl (atlastin) regulates mTor signaling and autophagy in Drosophila muscle through alteration of the lysosomal network. Autophagy. 2023;in press. https://doi.org/10.1080/15548627.2023.2249794 PMID: 37649246

14. Bernasconi N. Is epilepsy a curable neurodegenerative disease? Brain. 2016; 139(Pt 9):2336–7. https://doi.org/10.1093/brain/aww202 PMID: 27559105.

15. Roberson ED, Scearce-Levie K, Palop JJ, Yan F, Cheng IH, Wu T, et al. Reducing endogenous tau ameliorates amyloid beta-induced deficits in an Alzheimer's disease mouse model. Science. 2007; 316 (5825):750–4. https://doi.org/10.1126/science.1141736 PMID: 17478722.

16. Tai XY, Koepp M, Duncan JS, Fox N, Thompson P, Baxendale S, et al. Hyperphosphorylated tau in patients with refractory epilepsy correlates with cognitive decline: a study of temporal lobe resections. Brain. 2016; 139(Pt 9):2441–55. Epub 20160807. https://doi.org/10.1093/brain/aww187 PMID: 27497924.

17. Wu JW, Hussaini SA, Bastille IM, Rodriguez GA, Mrejeru A, Rilett K, et al. Neuronal activity enhances tau propagation and tau pathology in vivo. Nat Neurosci. 2016; 19(8):1085–92. Epub 20160620. https://doi.org/10.1038/nn.4328 PMID: 27322420.

18. Busche MA, Konnerth A. Neuronal hyperactivity—A key defect in Alzheimer's disease? Bioessays. 2015; 37(6):624–32. Epub 20150314. https://doi.org/10.1002/bies.201500004 PMID: 25773221.

19. Dickerson BC, Salat DH, Greve DN, Chua EF, Rand-Giovannetti E, Rentz DM, et al. Increased hippocampal activation in mild cognitive impairment compared to normal aging and AD. Neurology. 2005; 65 (3):404–11. https://doi.org/10.1212/01.wnl.0000171450.97464.49 PMID: 16087905.

20. Foran E, Trotti D. Glutamate transporters and the excitotoxic path to motor neuron degeneration in amyotrophic lateral sclerosis. Antioxid Redox Signal. 2009; 11(7):1587–602. https://doi.org/10.1089/ars.2009.2444 PMID: 19413484.

21. Naegele JR. Neuroprotective strategies to avert seizure-induced neurodegeneration in epilepsy. Epilepsia. 2007; 48 Suppl 2:107–17. https://doi.org/10.1111/j.1528-1167.2007.01071.x PMID: 17571357.

22. Ono T, Galanopoulou AS. Epilepsy and epileptic syndrome. Adv Exp Med Biol. 2012; 724:99–113. https://doi.org/10.1007/978-1-4614-0653-2_8 PMID: 22411237.

23. Rosenzweig M, Brennan KM, Tayler TD, Phelps PO, Patapoutian A, Garrity PA. The Drosophila ortholog of vertebrate TRPA1 regulates thermotaxis. Genes Dev. 2005; 19(4):419–24. Epub 20050128. https://doi.org/10.1101/gad.1278205 PMID: 15681611.

24. Summerville JB, Faust JF, Fan E, Pendin D, Daga A, Formella J, et al. The effects of ER morphology on synaptic structure and function in Drosophila melanogaster. J Cell Sci. 2016; 129(8):1635–48. https://doi.org/10.1242/jcs.184929 PMID: 26906425.

25. van der Graaf K, Srivastav S, Singh P, McNew JA, Stern M. The Drosophila melanogaster attP40 docking site and derivatives are insertion mutations of msp-300. PLoS One. 2022; 17(12):e0278598. Epub 20221214. https://doi.org/10.1371/journal.pone.0278598 PMID: 36516171.

26. Orso G, Pendin D, Liu S, Tosetto J, Moss TJ, Faust JE, et al. Homotypic fusion of ER membranes requires the dynamin-like GTPase atlastin. Nature. 2009; 460(7258):978–83. https://doi.org/10.1038/nature08280 PMID: 19633650.

27. Moss TJ, Andreazza C, Verma A, Daga A, McNew JA. Membrane fusion by the GTPase atlastin requires a conserved C-terminal cytoplasmic tail and dimerization through the middle domain. Proc Natl Acad Sci U S A. 2011; 108(27):11133–8. Epub 20110620. https://doi.org/10.1073/pnas.1105056108 PMID: 21690399.

28. Pulver SR, Pashkovski SL, Hornstein NJ, Garrity PA, Griffith LC. Temporal dynamics of neuronal activation by Channelrhodopsin-2 and TRPA1 determine behavioral output in Drosophila larvae. J Neurophysiol. 2009; 101(6):3075–88. Epub 20090401. https://doi.org/10.1152/jn.00071.2009 PMID: 19339465.

29. Lee M, Paik SK, Lee MJ, Kim YJ, Kim S, Nahm M, et al. Drosophila Atlastin regulates the stability of muscle microtubules and is required for synapse development. Dev Biol. 2009; 330(2):250–62. Epub 2009/04/04. https://doi.org/10.1016/j.ydbio.2009.03.019 [pii] PMID: 19341724.

30. Lee Y, Paik D, Bang S, Kang J, Chun B, Lee S, et al. Loss of spastic paraplegia gene atlastin induces age-dependent death of dopaminergic neurons in Drosophila. Neurobiol Aging. 2008; 29(1):84–94. Epub 2006/10/13. https://doi.org/10.1016/j.neurobiolaging.2006.09.004 PMID: 17030474.

31. Yagi R, Mayer F, Basler K. Refined LexA transactivators and their use in combination with the Drosophila Gal4 system. Proc Natl Acad Sci U S A. 2010; 107(37):16166–71. Epub 20100830. https://doi.org/10.1073/pnas.1005957107 PMID: 20805468.

32. Hamada FN, Rosenzweig M, Kang K, Pulver SR, Ghezzi A, Jegla TJ, et al. An internal thermal sensor controlling temperature preference in Drosophila. Nature. 2008; 454(7201):217–20. Epub 20080611. https://doi.org/10.1038/nature07001 PMID: 18548007.

33. Kirkhart C, Scott K. Gustatory learning and processing in the Drosophila mushroom bodies. J Neurosci. 2015; 35(15):5950–8. https://doi.org/10.1523/JNEUROSCI.3930-14.2015 PMID: 25878268.

34. Kaplan WD, Trout WE, 3rd. The behavior of four neurological mutants of Drosophila. Genetics. 1969; 61(2):399–409. https://doi.org/10.1093/genetics/61.2.399 PMID: 5807804.

35. Hartwig CL, Worrell J, Levine RB, Ramaswami M, Sanyal S. Normal dendrite growth in Drosophila motor neurons requires the AP-1 transcription factor. Dev Neurobiol. 2008; 68(10):1225–42. https://doi.org/10.1002/dneu.20655 PMID: 18548486.

36. Karunanithi S, Lin YQ, Odierna GL, Menon H, Gonzalez JM, Neely GG, et al. Activity-Dependent Global Downscaling of Evoked Neurotransmitter Release across Glutamatergic Inputs in Drosophila. J Neurosci. 2020; 40(42):8025–41. Epub 20200914. https://doi.org/10.1523/JNEUROSCI.0349-20.2020 PMID: 32928887.

37. Mosca TJ, Carrillo RA, White BH, Keshishian H. Dissection of synaptic excitability phenotypes by using a dominant-negative Shaker K+ channel subunit. Proc Natl Acad Sci U S A. 2005; 102(9):3477–82. Epub 20050222. https://doi.org/10.1073/pnas.0406164102 PMID: 15728380.

38. Vonhoff F, Kuehn C, Blumenstock S, Sanyal S, Duch C. Temporal coherency between receptor expression, neural activity and AP-1-dependent transcription regulates Drosophila motoneuron dendrite development. Development. 2013; 140(3):606–16. https://doi.org/10.1242/dev.089235 PMID: 23293292.

39. Bero AW, Yan P, Roh JH, Cirrito JR, Stewart FR, Raichle ME, et al. Neuronal activity regulates the regional vulnerability to amyloid-beta deposition. Nat Neurosci. 2011; 14(6):750–6. Epub 20110501. https://doi.org/10.1038/nn.2801 PMID: 21532579.

40. Cirrito JR, Yamada KA, Finn MB, Sloviter RS, Bales KR, May PC, et al. Synaptic activity regulates interstitial fluid amyloid-beta levels in vivo. Neuron. 2005; 48(6):913–22. https://doi.org/10.1016/j.neuron.2005.10.028 PMID: 16364896.

41. Mattson MP. Calcium and neurodegeneration. Aging Cell. 2007; 6(3):337–50. Epub 20070228. https://doi.org/10.1111/j.1474-9726.2007.00275.x PMID: 17328689.

42. Verma M, Wills Z, Chu CT. Excitatory Dendritic Mitochondrial Calcium Toxicity: Implications for Parkinson's and Other Neurodegenerative Diseases. Front Neurosci. 2018; 12:523. Epub 20180802. https://doi.org/10.3389/fnins.2018.00523 PMID: 30116173.